Tracking of Carotid Arteries in Ultrasound Images

Shubao Liu, Dirk Padfield, and Paulo Mendonca

GE Global Research, One Research Circle, Niskayuna, NY 12309
[lius,padfield,mendonca]@ge.com

Abstract. We introduce an automated method for the 3D tracking of carotids acquired as a sequence of 2D ultrasound images. The method includes an image stabilization step that compensates for the cardiac and respiratory motion of the carotid, and tracks the carotid wall via a shape and appearance model trained from representative images. Envisaging an application in automatic detection of plaques, the algorithm was tested on ultrasound volumes from 4,000 patients and its accuracy was evaluated by measuring the distance between the location of more than 4,000 carotid plaques and the location of the carotid wall as estimated by the proposed algorithm. Results show that the centroids of over 95% of the carotid plaques in the dataset were located within 3 mm of the estimated carotid wall, indicating the accuracy of the tracking algorithm.

1 Introduction

Cardiovascular disease (CVD) is the leading cause of death worldwide [23,2]. The availability of treatments that slow the progression of CVD increases the impact of early diagnosis in patient survival [4], and the presence of carotid plaque has been identified as a significant risk factor in the prognosis of CVD [9]. Due to its ease of use, accessibility, and safety, ultrasound (U/S) hold promise as tool for early detection of carotid plaque [15]. However, a full-blown ultrasound-based screening program for CVD would have a higher likelihood of success if the image-acquisition procedure could be performed by medical practitioners without the rigorous training requirements by sonographers and image readers reported in the literature [15], thereby providing an opportunity for computer-aided detection (CAD) systems.

A central component of an ultrasound-based CAD system for detection of carotid plaque is the accurate localization of the carotid wall. Multiple challenges must be overcome for the success of this task, including robustness to noise and anatomical variations, avoidance of other adjacent vascular structures, adequate disambiguation of the internal and external carotid arteries, and robustness to motion due to patient respiration, cardiac pulsation and, possibly, free-hand acquisitions.

The problem addressed in this paper is the tracking of the carotid in U/S images, with the express purpose of obtaining robust and accurate estimates of the carotid wall. In particular, the accurate localization of the carotid centerline [7,11] is of less importance, and therefore the problem can be recast as 3D carotid segmentation. This problem has been tackled under different imaging modalities, including coronary CT angiography (CTA) [6,22,20,13], MR [3,17,8], and U/S [5], as well as for different arteries, such as the coronaries [22,13,3] and the carotid [20,17,5]. Most commonly used segmentation

K. Mori et al. (Eds.): MICCAI 2013, Part II, LNCS 8150, pp. 526–533, 2013.

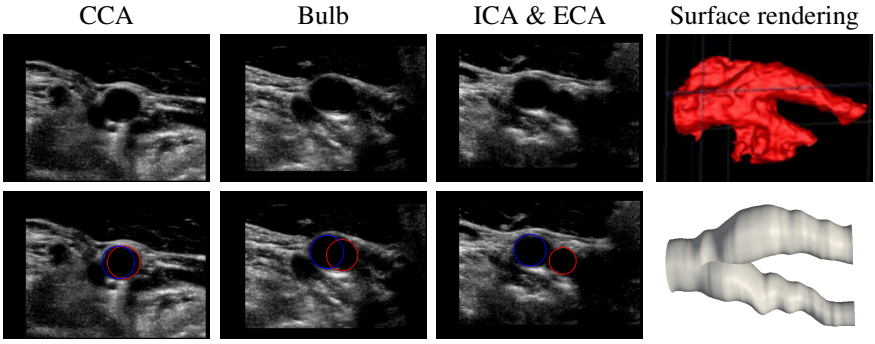

Fig. 1. 2D+time carotid images. The first three top image show the original images, and the first three bottom images show the same images with our carotid wall tracking overlaid. The last top image shows the carotid reconstructed from a level set segmentation. The last bottom image shows the carotid reconstructed from our tracking algorithm.

methods include level-set segmentation [19], snakes [16], and region growing [1]. Most of the methods are variants of the level-set method, which work well in CT and MR imaging modalities where the image of the artery walls is in a sharp contrast with the background tissue.

Typical ultrasound systems, however, yield images of much lower contrast and higher levels of noise compared to CT and MR. Fig. 1 shows the loss of contrast of the carotid wall and the blurring of lumen commonly observed in ultrasound images. Since the artery boundary may not be clearly visible, the segmentation of the artery in such images is a challenging problem. The top right image of this figure shows results of applying a level-set segmentation method [24] on one typical image. It can be seen that the segmentation is not satisfactory in either its depiction of the general geometry of the artery nor in the accuracy of the localization of the carotid wall. The imaging quality and strong local ambiguities are an obstacle to general segmentation algorithms that rely on image intensity and region boundaries. Therefore, the majority of U/S-based carotid segmentation methods have been limited to: 2D longitudinal views [12], the common carotid artery region [14,21], or method that are only semi-automatic [18].

The contributions of this paper are: a fully automated model-based method for tracking of vasculature that is effective under poor imaging conditions; the use of repulsive forces in simultaneous trackers to handle bifurcations and topological alterations of the tracked path; the use of an image stabilization method for hand-held 3D ultrasound data that allows for tracking even when the path of the ultrasound probe deviates from a straight line.

2 Methods

Our approach consists of three key steps: image stabilization through inter-frame registration, generation of a 2D canonical appearance model for the carotid cross section, and model-based tracking. In the sections that follow we make reference to the anatomical subdivisions of the carotid. Following the direction of blood flow, the main branch

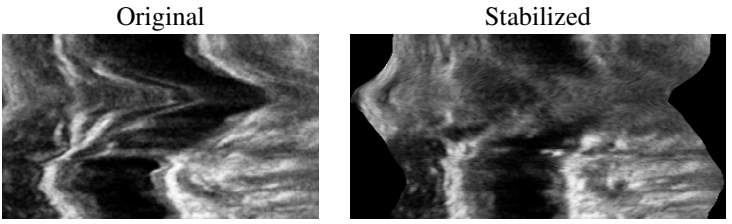

Fig. 2. Result of image stabilization. In the original image, the lumen moves in a winding path, likely due to the hand movement of the sonographer. The image stabilization yields a volume with more rectilinear structures. The black regions on the right and left of this image show how the image is shifted to produce a better alignment.

of the carotid is the common carotid artery (CCA), followed by the bulb, which is a enlarged region containing the bifurcation. The carotid then branches into the external and internal carotid arteries (ECA and ICA, resp.).

2.1 Image Stabilization

To stabilize the relative motion between the U/S probe and the carotid, we use a masked FFT registration algorithm [10], limited to translational motion, to register selected pairs of 2D slices. Since the anatomy changes gradually in 3D, the image content in adjacent slices include a significant amount of overlap even though they are imaging different regions. Clearly, the motion of the carotid between acquisition of adjacent frames is not simply translational, but this simple model is sufficient as an image stabilization step prior to tracking, and more complicated motion models are not necessary in our application. Translations from pairwise registrations are accumulated over the z dimension to compute the transform of every slice back to the original slice.

In practice, registering adjacent slices does not work robustly because the acquisition is so fast that the typical motion from frame to frame is of only a fraction of a pixel. Therefore, rather that carrying out a subpixel registration, which would also require image interpolation and leads to drift over time, we register 2D images that are h frames apart. Considering that the component of highest frequency in the carotid motion is due to cardiac pulsation, for an acquisition at 30 frames per second we set h to 10, so that the registered images will still be within the same cardiac cycle. The translation computed in this way is then interpolated across the intervening slices. This procedure has the additional advantage of decreasing the computation time of the image stabilization process, since for a 3D sequence with N slices only N/h registrations are required.

An illustrative result of the image stabilization procedure is shown in Figure 2. In the original view, the central portion of the lumen winds to the right and then back. In the stabilized volume the lumen follows a more rectilinear path. Furthermore, whereas in the original image the probe followed the CCA into one of its branches after the bulb, in the stabilized volume the bifurcation is clearly shown as an interruption in the rectilinear path of the carotid.

2.2 Carotid Tracking

Given the stabilized images, the next step is to extract the carotid artery walls from the sequence of 2D ultrasound images. The goal here is not only to track the centerline of the carotid but also to obtain a good approximation of the location of the wall, which is the region of interest for plaque detection. Carotid arteries transport blood at a high pressure, and their cross section is very close to circular. The use of cylindrical models with circular cross-sections has been used to detect vessel centerlines in both CT and US images [7,11]. We formulate the carotid wall tracking problem as a two-circle tracking problem using a geometric and appearance approximation to the carotid anatomy model. Initially, in the CCA region, these two circles are very close to each other. As the probe moves to the bulb region, these two circles, influenced by a repulsive force, separate to model the artery junction: the bulb region is modeled as the convex hull of two circles. Past the bulb, the circles will be completed separated to model ICA and ECA.

Initialization. Unlike other approaches in the literature, our algorithm is fully automatic — we could not have applied it to over 4,000 U/S volumes otherwise. To automatically find the artery in the first few slices, which are in the CCA region, we use a template matching approach. We generate the template by taking 100 arteries manually cropped, translated, and scaled, as shown in the left image of Fig. 3. The intensities of these registered images are then averaged at each pixel, resulting in the center of Fig. 3. An initial center and radius for the tracking circles is then obtained through a simple exhaustive template matching of this model against the first few frames of each input U/S volume.

It seems reasonable to attempt to proceed with this "tracking through detection" approach along the remaining of the carotid. However, because of strong artifacts, such as lateral and posterior shadows, as well as anatomical variations and the presence of adjacent vasculature, particularly the jugular, this model is too rigid to accomodate the changes in appearance observed throughout the carotid. Instead, we further simplify the model, preserving only its radial properties and ignoring tangential variability. To achieve that, we start from the average model in the center of Fig. 3. We generate a radial profile model by averaging all profiles emanating from the center of the averaged carotid, resulting in the single profile shown on the right of Fig. 3. This converts the model into a descriptive 1D profile $\rho_0(r)$ that can be easily compared against their counterparts $\rho_i(r/R_i)$ in slice i of a input carotid volume for each value of the parameter $\theta_i = (x_i, y_i, R_i)$, where (x_i, y_i) is the putative center of the carotid on slice i, and R_i is the putative carotid radius. Observe that $\rho_i(r)$ is computed in exactly the same way as $\rho_0(r)$, i.e., by computing the average intensity profile at frame i of a given volume, but with profiles emanating from some position (x_i, y_i). The term R_i in $\rho_i(r/R_i)$ for a some radius R_i results in a scaling of the profile $\rho_i(r)$.

For a given θ_i, we now define a likelihood term given by

$$L(I_i|\theta_i) = \exp(-\sum_r (\rho_i(r/R_i) - \rho_0(r))^2). \quad (1)$$

Incorporating slice-to-slice smoothness constraints, we obtain a term corresponding to a posterior, given by

$$L(\theta_i|I_i, \theta_{i-1}) = L(I_i|\theta_i) \exp(-\alpha||\theta_i - \theta_{i-1}||^2), \quad (2)$$

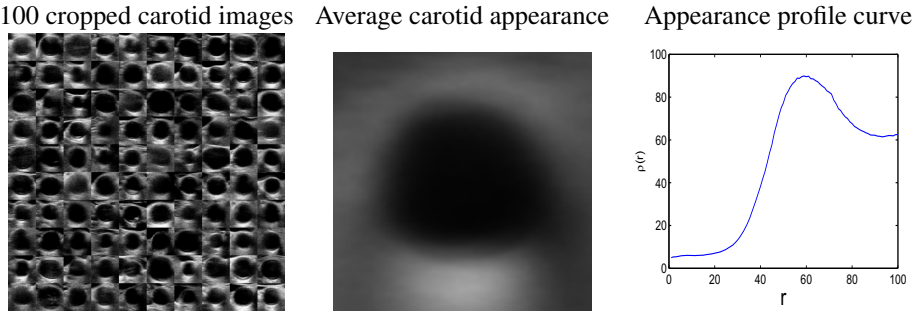

Fig. 3. Carotid appearance model. The left shows 100 representative carotid images that are averaged to create the appearance model in the middle. The right shows the appearance profile from averaging the middle image radially.

where α is the parameter controlling the amount of smoothness we enforce on the tracking trajectory.

The described formulation is suitable for modeling CCA region, which can be approximated by a single circle. Next, we extend the formulation to modeling bifurcation (e.g., bulb) and two branches (e.g., ICA, ECA), by tracking two circles simultaneously and modeling their interactions. Let's denote the two carotid parameters in frame i by θ_i^1 and θ_i^2. Then the likelihood of tracking these two circles simultaneously but independently can be written simply as the product of their individual likelihood functions, that is, $L(\theta_i^1, \theta_i^2 | I_i, \theta_{i-1}^1, \theta_{i-1}^2) = L(\theta_i^1 | I_i, \theta_{i-1}^1) L(\theta_i^2 | I_i, \theta_{i-1}^2)$. However this straightforward formulation has a degenerate solution, where these two circles follows exactly the same trajectory. The missing element is a repulsive interaction that forces divergence in the trajectories *when supported by the data, i.e., around and beyond the carotid bifurcation*. We model this interaction as

$$\phi(\theta_i^1, \theta_i^2) = \exp(\lambda(||x_i^1 - x_i^2||^2 + ||y_i^1 - y_i^2||)). \tag{3}$$

The parameter λ controls the range of force, and is chosen empirically through experiments. The interaction force is strong when two circles are close, and it becomes exponentially weaker when they are separated further. Putting all the above components together results in our final carotid tracking formulation

$$L(\theta_i^1, \theta_i^2 | \theta_{i-1}^1, \theta_{i-1}^2) = L(\theta_i^1 | I_i, \theta_{i-1}^1) L(\theta_i^2 | I_i, \theta_{i-1}^2) \phi(\theta_i^1, \theta_i^2). \tag{4}$$

The optimal circle trajectories are tracked for all frames in a sequential order by exhaustive search over a small range of values for θ_i centered at θ_{i-1}.

3 Results

We hold a dataset with 4,000 U/S volumes with plaque locations annotated by expert cardiologists. The datasets were acquired in distinct geographic locations and multiple

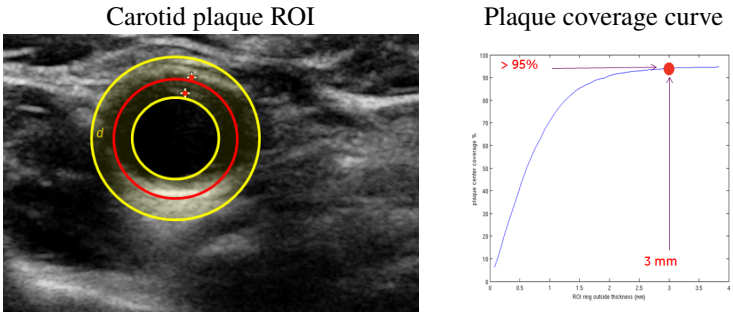

Fig. 4. Plaque coverage ROI and coverage curve. The red curve in (a) shows the tracked circle at a plaque location, the yellow circles indicate a distance of 3mm from the tracked wall, and the two red markers indicate the location of the inner and outer walls of a plaque manually annotated by a cardiologist. The coverage curve in (b) plots the number of markers that are within a certain distance from the tracked circle. In particular, 95% of all of the 4124 plaque centroids fall within 3 mm from the carotid wall.

U/S systems and operators, always with a hand-held probe. The future goal of our work is the development of automated algorithms for detection of plaque in U/S, and our validation approach is targeted towards this goal: We focus our validation efforts on determining how close our tracked carotid is to ground-truth plaque locations. Choosing small region around the tracked carotid then serves as an accurate way to restrict the search space for later plaque detection approaches, which is an important application enabled by accurate carotid tracking.

For a single set of algorithm parameters, Fig. 4 shows the cumulative distribution of distances of 4124 plaque centroids to the carotid wall as estimated by our algorithm, indicating that over 95% of all plaques are detected within 3 mm of a tracked circle. This distance is clinically relevant, because current clinical protocol indicate that a thickening of the carotid wall of 1.5 mm or more is considered to be plaque.

Fig. 5 illustrates the proposed algorithm's capabilities to handle tracking on challenging carotid regions. The rightmost column shows tracking results in the CCA region, where the tracked circles nearly overlap. The second column shows results in the bulb region, after which the tracked circles completely separate into the ECA and ICA, as shown in the third column. Rendered volumes produced from the tracked circles are shown in the leftmost column of Fig. 5.

4 Conclusions

We presented algorithms for robustly localizing carotid artery walls in low-quality U/S scans. An image stabilization method is proposed to compensate for probe jitter. A carotid tracking method using prior information for carotid geometry and appearance was introduced, in combination with the temporal information to segment carotid arteries from low-contrast, noisy ultrasound images. Together, these methods enable large-scale carotid artery analysis with safe and low-cost U/S imaging. The carotid artery

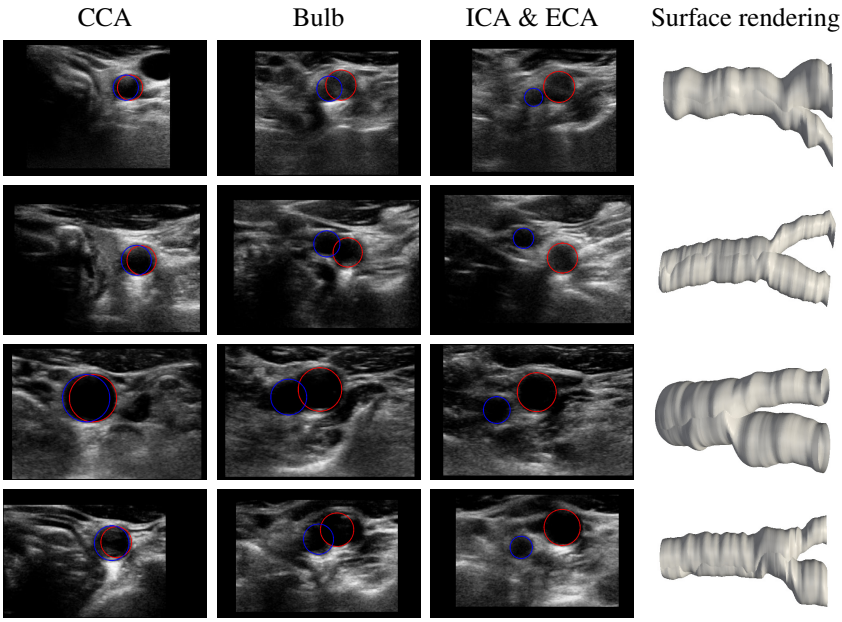

Fig. 5. Tracking results in different carotid regions. The tracked circles almost completely overlap in the CCA region (first column), and still show reasonable amount of overlap in the bulb (second column), after which they completely separate, due to an external repulsive force, into the ECA and ICA (third column). Illustrative 3D renderings of the tracks are shown on the left.

wall segmentation results and the plaque distribution obtained from over 4,000 patients provide a solid foundation for further research on automatic plaque detection and quantification leading to cardiovascular disease risk assessment.

References

1. Abdel-Dayem, A.R., El-Sakka, M.R.: Carotid artery ultrasound image segmentation using fuzzy region growing. In: Kamel, M.S., Campilho, A.C. (eds.) ICIAR 2005. LNCS, vol. 3656, pp. 869–878. Springer, Heidelberg (2005)
2. American Heart Association: Heart disease and stroke statistics – 2012 update: A report from the american heart association. Circulation 125, 188–197 (2012)
3. Cline, H.E., Thedens, D.R., Irarrazaval, P., Meyer, C.H., Hu, B.S., Nishimura, D.G., Ludke, S.: 3D MR coronary artery segmentation. MRM 40, 697–702 (1998)
4. Cohn, J.N.: Arterial stiffness, vascular disease, and risk of cardiovascular events. Circulation 113, 601–603 (2006)
5. Delsanto, S., Molinari, F., Giustetto, P., Liboni, W., Badalamenti, S., Suri, J.S.: Characterization of a completely user-independent algorithm for carotid artery segmentation in 2-D ultrasound images. IEEE Trans. on Instrumentation and Measurement 56(4), 1265–1274 (2007)
6. Hameeteman, K., Freiman, M., et al.: Carotid lumen segmentation and stenosis grading challenge. MIDAS Journal (March 2010)

7. Krissian, K., Ellsmere, J., Vosburgh, K., Kikinis, R., Westin, C.F.: Multiscale segmentation of the aorta in 3D ultrasound images. In: Proc. Engineering in Medicine and Biology Society., vol. 1, pp. 638–641 (2003)
8. Lekadir, K., Yang, G.Z.: Carotid artery segmentation using an outlier immune 3D active shape models framework. In: Larsen, R., Nielsen, M., Sporring, J. (eds.) MICCAI 2006. LNCS, vol. 4190, pp. 620–627. Springer, Heidelberg (2006)
9. Muntendam, P., McCall, C., Sanz, J., Falk, E., Fuster, V.: The BioImage study: Novel approaches to risk assessment in the primary prevention of atherosclerotic cardiovascular disease — Study design and objectives. American Heart Journal 160(1), 49–57 (2010)
10. Padfield, D.: Masked object registration in the Fourier domain. IEEE Transactions on Image Processing 21(5), 2706–2718 (2012)
11. Pock, T., Beichel, R., Bischof, H.: A novel robust tube detection filter for 3D centerline extraction. In: Kalviainen, H., Parkkinen, J., Kaarna, A. (eds.) SCIA 2005. LNCS, vol. 3540, pp. 481–490. Springer, Heidelberg (2005)
12. Rossi, A.C., Brands, P.J., Hoeks, A.P.: Automatic recognition of the common carotid artery in longitudinal ultrasound B-mode scans. Medical Image Analysis 12(6), 653–665 (2008)
13. Scherl, H., Hornegger, J., Prümmer, M., Lell, M.: Semi-automatic level-set based segmentation and stenosis quantification of the internal carotid artery in 3D CTA data sets. Medical Image Analysis 11(1), 21–34 (2007)
14. Slabaugh, G., Unal, G., Fang, T., Wels, M.: Ultrasound-specific segmentation via decorrelation and statistical region-based active contours. In: CVPR, vol. 1, pp. 45–53 (June 2006)
15. Stein, J.H., et al.: Use of carotid ultrasound to identify subclinical vascular disease and evaluate cardiovascular disease risk: A consensus statement from the American Society of Echocardiography Carotid Intima-Media Thickness Task Force endorsed by the Society for Vascular Medicine. Journal of the American Society of Echocardiography 21(2), 93–111 (2008)
16. Terzopolous, D., Witkin, A., Kass, M.: Snakes: Active contour models. Int. Journal of Computer Vision 1(4), 211–221 (1987)
17. Thomas, J.B., Antiga, L., Che, S.L., Milner, J.S., Steinman, D.A., Spence, J.D., Rutt, B.K., Steinman, D.A.: Variation in the carotid bifurcation geometry of young versus older adults – Implications for geometric risk of atherosclerosis. Stroke 36(11), 2450–2456 (2005)
18. Ukwatta, E., Awad, J., Ward, A.D., Buchanan, D., Samarabandu, J., Parraga, G., Fenster, A.: Three-dimensional ultrasound of carotid atherosclerosis: Semiautomated segmentation using a level set-based method. Med. Phys. 38(5), 2479–2493 (2011)
19. Ukwatta, E., Awad, J., Ward, A., Buchanan, D., Parraga, G., Fenster, A.: Coupled level set approach to segment carotid arteries from 3D ultrasound images. In: ISBI, pp. 37–40 (2011)
20. Vukadinovic, D.: Carotid artery segmentation and plaque quantification in CTA. In: ISBI (2009)
21. Waelkens, P., Ahmadi, S.-A., Navab, N.: Frangi goes US: Multiscale tubular structure detection adapted to 3D ultrasound. In: Ayache, N., Delingette, H., Golland, P., Mori, K. (eds.) MICCAI 2012, Part I. LNCS, vol. 7510, pp. 625–633. Springer, Heidelberg (2012)
22. Wang, C., Smedby, O.: An automatic seeding method for coronary artery segmentation and skeletonization in CTA. The Insight Journal (2008)
23. The Top Ten Causes of Death (June 2011), `http://www.who.int/mediacentre/factsheets/fs310/en/index2.html`
24. Yushkevich, P.A., Piven, J., Cody Hazlett, H., Gimpel Smith, R., Ho, S., Gee, J.C., Gerig, G.: User-guided 3D active contour segmentation of anatomical structures: Significantly improved efficiency and reliability. Neuroimage 31(3), 1116–1128 (2006)